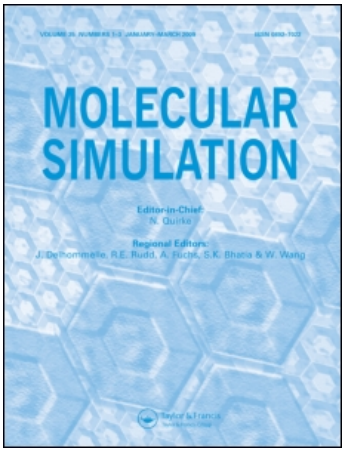

Molecular Simulation
Publication details, including instructions for authors and subscription information:
http://www.informaworld.com/smpp/title~content=t713644482

A comparison of model linear chain molecules with constrained and flexible bond lengths under planar Couette and extensional flows

Thomas A. Hunt[a]; B. D. Todd[a]
[a] Centre for Molecular Simulation, Swinburne University of Technology, Hawthorn, Victoria, Australia

To cite this Article Hunt, Thomas A. and Todd, B. D.(2009) 'A comparison of model linear chain molecules with constrained and flexible bond lengths under planar Couette and extensional flows', Molecular Simulation, 35: 14, 1153 — 1167
To link to this Article: DOI: 10.1080/08927020902912295
URL: http://dx.doi.org/10.1080/08927020902912295

Molecular Simulation
Vol. 35, No. 14, December 2009, 1153–1167

Taylor & Francis
Taylor & Francis Group

A comparison of model linear chain molecules with constrained and flexible bond lengths under planar Couette and extensional flows

Thomas A. Hunt[1] and B.D. Todd*

Centre for Molecular Simulation, Swinburne University of Technology, Hawthorn, Victoria, 3122, Australia

(*Received 27 January 2009; final version received 17 March 2009*)

We compare directly under flow two commonly used coarse grained models of linear polymers, namely the flexible *finitely extensible nonlinear elastic* (FENE) chain, and the *freely jointed tangent sphere chain*, otherwise known as the *freely jointed chain*. The comparison is based on viscometric, structural and dynamical properties. We use non-equilibrium molecular dynamics to simulate steady-state systems under planar Couette flow and planar extensional flow. Computed properties include shear and elongational viscosities, normal stresses, radius of gyration and end-to-end distances, order parameters, alignment angles and spin angular velocities. In all computed properties we observe very little difference between the two molecular models. Therefore, the choice of either model is suitable, though there is a computational advantage in the use of the FENE model.

Keywords: non-equilibrium molecular dynamics; shear flow; elongational flow; polymer melts; FENE chain

1. Introduction

There are many molecular potentials available for simulating polymeric liquids. Despite this large collection, we should also acknowledge that many of the properties of polymeric liquids are independent of the specific molecule being investigated. In this paper, we compare some of the rheological and structural properties of two commonly used molecular models, commonly known as the *finitely extensible nonlinear elastic* molecule (FENE) and the *freely jointed chain* molecule (FJC). The first of these (FENE) consists of Lennard-Jones (LJ) atoms connected by a finitely extensible nonlinear spring force. The second again consists of LJ atoms, however a constraint force is used to fix the bond length between the atoms.

Gauss' principle of least constraint [1] has been used to simulate molecules with constrained bond length and bond angles [2,3] and has been used for the simulation of both linear and branched molecules. This constraint algorithm can be used to generate so-called 'tangent chains' of LJ atoms. Such tangent chains have been studied for their equilibrium equation of state properties [4] and also quite extensively for non-equilibrium molecular dynamics (NEMD) rheological properties [5–9]. The model has also been used to simulate linear molecules in solution [10,11] as well as polymer melts containing spherical filler particles [12].

Matin et al. [5] performed the first NEMD simulations of small molecules using the Kraynik Reinelt [13–16] periodic boundary conditions (PBCs) for planar extensional flow (PEF) and the molecular SLLOD algorithm [2,17]. This model consisted of LJ dimers bonded using the Gaussian constraint algorithm [18–21]. These simulations confirmed that under PEF, molecules have zero average spin angular velocity, a quantity which had been measured under planar Couette flow (PCF) in previous publications. In addition to the chlorine molecules Matin et al. [5] simulated liquids of LJ atoms as well as two-site and four-site FJC molecules. It was confirmed that the atomic systems had little elasticity since the first normal stress ($N_1 = P_{yy} - P_{xx}$) was found to be approximately zero, except at the highest strain rate. For molecular systems it was found that N_1 deviated significantly from zero as the strain rate increased and was attributed to the elasticity of the molecular fluid [22]. Further, results for the two-site FJC molecules [6] found that independent calculation for PCF and PEF of the coefficients of the third order retarded motion expansion led to consistent results. Examination of the conditions for which the ratio $\eta_1/\eta_2 \approx 0$ led the authors to conclude that the Newtonian regime extended to $\dot{\varepsilon} = 0.0296$. This was in agreement with their plot of viscosity against strain rate.

Subsequent simulations of longer FJC molecules found [7–9] that lower order coefficients for the RME were in agreement when calculated using data from PCF and PEF. However, it was found that the higher order terms did not have the same level of agreement. This was attributed to large uncertainties in the results for longer molecules at low strain rates. Calculation of the N_s dependence (number of sites per molecule) of η_0 and the zero strain rate first

*Corresponding author. Email: btodd@swin.edu.au

ISSN 0892-7022 print/ISSN 1029-0435 online

DOI: 10.1080/08927020902912295
http://www.informaworld.com

normal stress $\Psi_{1,0}$ agreed with the Rouse model predictions that $\eta_0 \propto N_s$ and $\Psi_{1,0} \propto N_s^3$.

Improvement on these results [9], where chain lengths of up to $N_s = 100$ were simulated, showed agreement between calculated coefficients of the RME for terms up to second order in the strain rate. Disagreement was found in the third order terms calculated from the normal stress coefficients of PEF η_1 and η_2. It was suggested that this discrepancy was due to a mismatch between the assumptions of the RME and the conditions of the simulation.

Several significant studies have used the FENE model to investigate rheological properties of polymer melts. Kröger et al. [23] investigated rheological and structural properties of a monodisperse FENE melt under PCF with molecules between $N_s = 10-100$ in length. These simulations used a velocity re-scaling algorithm and it is not clear whether this algorithm led to over alignment in the system that had been observed in other molecular simulations [19]. However, the range of data presented in this work is very significant. Two methods were used to calculate the structure of the liquid: firstly the alignment tensor was calculated, and through this the alignment angle of molecules. Secondly, the structure factor was calculated and compared favourably with experimental results from small angle neutron scattering experiments [24]. Comparing the alignment tensor and the stress tensor confirmed the stress-optic law in the Newtonian regime. It was shown that the Rouse prediction for the chain-length dependence of the viscosity $\eta_0 \propto N_s$ was confirmed for chains of length $N_s \leq 60$, with a slight up-turn in this curve for $N_s = 100$, suggesting that the crossover between the Rouse and reptation regime had been reached. This last observation was confirmed by Kröger and Hess [25] in a publication which presented steady state viscosities of monodisperse FENE systems ranging in length from $N_s = 10$ up to $N_s = 400$. A similar conclusion was reached by Bosko et al. [26].

In the case of extensional flows, Kröger et al. [27] investigated the start-up of uniaxial extensional flow (UEF) and subsequent relaxation. The authors compared experimental observations of molecular alignment and stress measurements with similar measurements from NEMD simulation. These measurements allowed them to determine the range of validity of the stress-optic law, the linear relationship between the stress and alignment of bond vectors in the liquid. In the start-up phase of the simulations and experiments, they found that the stress-optic law was valid at low strain-rates and at high temperatures. However, in the relaxation phase it was found that the rule was valid for all systems. At high strain-rates a stress offset was observed which was found to have a linear dependence on the strain-rate. Baig et al. [28] and Kim et al. [29] have also performed NEMD simulations under PEF but using a modified form of the Siepmann–Karaboni–Smit united-atom model for linear alkanes [30]. As the model used in this case is different than either the FENE or FJC models, we do not consider direct comparisons with our work.

Bosko et al. [26,31,32] have performed simulations under PCF of dendrimer liquids where the molecules were composed of beads connected by the same FENE potential that we have used in our study. They have compared their results with simulations of linear FENE molecules.

Several authors have used Brownian dynamics simulations to investigate the effect of molecular properties on the mobility of FENE molecules as well as structural properties of model polymer melts at equilibrium. These authors employed the technique that had been used by Grest and Kremer [33,34] in their investigations of Rouse and reptative dynamics.

Faller et al. [35,36] have used the FENE molecular potential combining it with a three-body torsional potential to determine the effect of chain stiffness and chain length on the reorientation times of chain segments. They found that there were two processes: a short-time reorientation process which followed a power law relation and a second long-time reorientation process which followed an exponential relation. Both these processes were strongly affected by the chain stiffness and the chain length. In contrast, it was found that the local structure of the melt was not changed greatly by variation in the parameters of the molecule.

Using the same Brownian dynamics technique, with a harmonic bond potential rather than a FENE and torsional potential, Abrams and Kremer [37,38] investigated confined and bulk systems of linear molecules, where the ratio of bond length to the bead diameter l_0/d_0 was varied. They found that as the bond length increased when compared with the bead diameter, there was an increase in the pressure and surface tension. By examining the local structure of the fluid by calculating radial distribution functions, Abrams and Kremer found that the local ordering in the fluid was enhanced by an increase in the ratio l_0/d_0. They used this to explain the increase in macroscopic variables. In the subsequent paper [38] where the correlation functions of the Rouse modes were investigated, they found that when the ratio l_0/d_0 was doubled there was a 20-fold increase in the monomer friction coefficient ζ. This was again attributed to the increase in local ordering in the fluid.

In this paper, we will present and discuss results from NEMD simulations of FJC and FENE molecules undergoing both planar shear and elongational flows. The basis of comparison will be the commonly calculated steady state rheological properties, such as viscosities and normal stresses, along with some structural properties which can be readily calculated in molecular simulations. We present the simulation algorithms and techniques used for the study, computational detail, a summary of the length of

simulations etc. along with necessary details of how averages were calculated. Greater details can be found in the PhD thesis of Hunt [39].

From the outset, there are several reasons for making the comparison of the FENE and FJC molecules. Firstly, we wish to investigate the effect that the flexibility of the bond length of the FENE molecules has on the macroscopic properties of the melt. Secondly, the force calculation for the FENE molecule is less involved than the constraint algorithm used for the simulation of FJC molecules and so it is worthwhile comparing the computational efficiency of the two models. Thirdly, the data presented in this paper are rheological and structural and will be followed up in a subsequent paper with an analysis of self-diffusion of molecules in shear and extensional flows. To our knowledge, diffusion for polymer melts experiencing PEF has not yet been attempted for either molecular model using NEMD methods.

In Section 2, we present a summary of the simulation algorithm and follow it in Section 3 with further simulation details. In Section 4, we present analysis of the average bond length of the FENE systems and use this data to make a choice of the bond length for the FJC systems. Section 5 presents the results from the simulations we have performed, which include viscoelastic, dynamic and structural properties, and we make some concluding remarks in Section 6.

2. Molecular models and simulation algorithm

2.1 Molecular models

The FENE molecules that we simulate here consist of a linear chain of N_s beads interacting via pair potentials. Adjacent beads along the chain interact via a combined FENE spring potential and Weeks–Chandler–Andersen (WCA) potential [40], discussed below. Beads which are not on the same molecule and beads which *are* on the same molecule but not adjacent interact just by the WCA potential. For two adjacent beads separated by the vector $\mathbf{r}_{ij}$, the FENE contribution to their interaction is,

$$U_{ij}^{\mathrm{FENE}} = \begin{cases} -\frac{1}{2}kR_0^2 \ln\left[1-\left(\frac{r_{ij}}{R_0}\right)^2\right] & \text{for } r_{ij} \le R_0 \text{ and} \\ +\infty \quad \text{for } r_{ij} \ge R_0 \end{cases}, \tag{1}$$

where $k = 30\varepsilon_{\mathrm{LJ}}$ is the spring constant for the FENE bond (in a similar way to the Hookean spring constant), $R_0 = 1.5\sigma_{\mathrm{LJ}}$ is the limit to the bond extension (see Figure 1), and $r_{ij} = |\mathbf{r}_j - \mathbf{r}_i|$ is the distance between particles i and j. The importance of the FENE potential over a Hookean potential is that a FENE bond cannot be extended beyond the fixed length $R_0 = 1.5\sigma_{\mathrm{LJ}}$. A plot of the potential between adjacent beads is given in Figure 1. Note that, the potential has a minimum close to $r_{ij} = 1.0\sigma_{\mathrm{LJ}}$. The choice

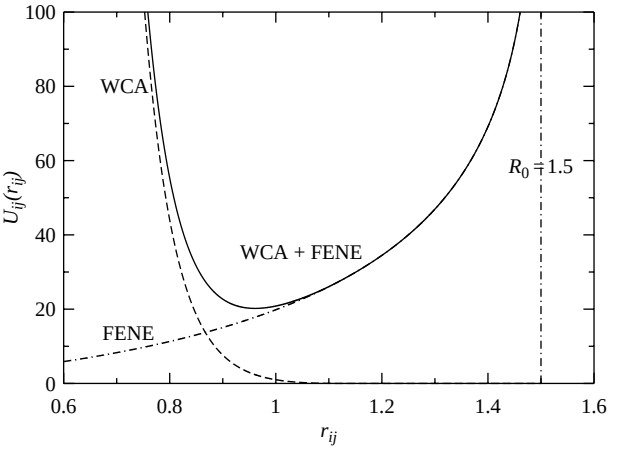

Figure 1. A comparison of the FENE and WCA potentials, and their sum.

of coefficients k and R_0 are the values that have been used in a number of previous investigations using this potential [23,25–27,31,41]. It has been reported by the authors in these works that the molecules did not cross each other. Thus, a key property of the polymers was correctly modelled.

Two very common interatomic potentials are the LJ potential and the WCA potential mentioned above [40]. Both potentials are isotropic ($U(\mathbf{r}_i, \mathbf{r}_j) = U(|\mathbf{r}_j - \mathbf{r}_i|) \equiv U(r_{ij})$ and the full LJ potential has the following form,

$$U_{ij}^{\mathrm{LJ}}(r_{ij}) = 4\varepsilon_{\mathrm{LJ}}\left[\left(\frac{\sigma_{\mathrm{LJ}}}{r_{ij}}\right)^{12} - \left(\frac{\sigma_{\mathrm{LJ}}}{r_{ij}}\right)^{6}\right], \tag{2}$$

where σ_{LJ} and $\varepsilon_{\mathrm{LJ}}$ are the effective atomic diameter and well depth, respectively. The WCA potential is essentially the repulsive part of the LJ potential and consequently has a cut-off radius at the LJ minimum $r_c = 2^{1/6}\sigma_{\mathrm{LJ}}$.

$$U_{ij}^{\mathrm{WCA}}(r_{ij}) = \begin{cases} 4\varepsilon_{\mathrm{LJ}}\left[\left(\frac{\sigma_{\mathrm{LJ}}}{r_{ij}}\right)^{12} - \left(\frac{\sigma_{\mathrm{LJ}}}{r_{ij}}\right)^{6}\right] - U_c & \text{for } r_{ij} \le r_c \text{ and} \\ 0 \quad \text{for } r_{ij} \ge r_c \end{cases}, \tag{3}$$

where, $U_c = U_{ij}^{\mathrm{LJ}}(r_c)$. The WCA potential is shown in Figure 1, together with the FENE potential which is used for molecular bonding.

We have also simulated linear molecules with constrained bond lengths, namely the freely jointed tangent chain (FJC). The Gaussian constraint method used to calculate the constraint force is presented in works by Edberg et al. [2,17] and by Morriss and Evans [3]. In addition to the constraint force, the short ranged and repulsive WCA potential is imposed between atoms on

different chains and between atoms on the same chain which are not adjacent. In previous works [5,6,8,9] the bond length had been constrained to $b = 1.0\sigma_{\mathrm{LJ}}$. In this work however, we have constrained the bond length to $b = 0.97\sigma_{\mathrm{LJ}}$. This corresponds to the average of the bond length of the FENE molecule at equilibrium (for $T = 1.0$, $\rho = 0.84$). Further discussion of this choice of bond length is given in what follows.

We note here that the names we use for these models have been used in the past to nominate other molecular models which differ from those used here. In particular, the term 'freely-jointed-chain' is commonly used to denote any model in which the bond angles are free to have any orientation. Furthermore, the FENE potential is commonly used to denote dimers and chains which just use the potential as given in (1) without the inclusion of the repulsive contribution from the WCA potential. Our discussion above makes is clear exactly which two models we are comparing.

2.2 Equations of motion

Apart from the molecular model used in these simulations, the equations of motion used in our simulations are the same. The SLLOD equations of motion that we use here for molecular systems are given by [2,17,42]:

$$\dot{\mathbf{r}}_{i\alpha} = \frac{\mathbf{p}_{i\alpha}}{m_{i\alpha}} + \mathbf{r}_i \cdot \nabla \mathbf{u}, \tag{4}$$

$$\dot{\mathbf{p}}_{i\alpha} = \mathbf{F}_{i\alpha}^{\mathrm{LJ}} + \mathbf{F}_{i\alpha}^{\mathrm{C/FENE}} - \frac{m_{i\alpha}}{M_i}\mathbf{p}_i \cdot \nabla \mathbf{u} - \zeta_M \frac{m_{i\alpha}}{M_i}\mathbf{p}_i. \tag{5}$$

This is the so-called 'molecular SLLOD' implementation. The subscript $i\alpha$ denotes site α on molecule i. $\mathbf{r}_{i\alpha}, (\mathbf{p}_{i\alpha}, m_{i\alpha})$ is the position (momentum, mass) of the designated site. The force on a site is separated into two terms; $\mathbf{F}_{i\alpha}^{\mathrm{LJ}}$ is the contribution due to the LJ interaction and $\mathbf{F}_{i\alpha}^{\mathrm{C/FENE}}$ is either the constraint force for a FJC system or the bonding force for the FENE system. M_i is the mass of molecule i, and ζ_M is the molecular thermostat multiplier. $\mathbf{r}_i = (r_{xi}, r_{yi}, r_{zi})$ and $\mathbf{p}_i = (p_{xi}, p_{yi}, p_{zi})$ are the centre of mass and momentum of molecule i, given as:

$$\mathbf{r}_i = \frac{\sum_{\alpha=1}^{N_s} m_{i\alpha}\mathbf{r}_{i\alpha}}{\sum_{\alpha=1}^{N_s} m_{i\alpha}}, \tag{6}$$

$$\mathbf{p}_i = \sum_{\alpha=1}^{N_s} \mathbf{p}_{i\alpha} \tag{7}$$

and the molecular thermostat is

$$\zeta_{\mathrm{M}} = \frac{\sum_{i=1}^{N_m} (\mathbf{F}_i \cdot \mathbf{p}_i - \mathbf{p}_i \cdot \nabla \mathbf{u} \cdot \mathbf{p}_i)/M_i}{\sum_{i=1}^{N_m} \mathbf{p}_i^2/M_i}. \tag{8}$$

The streaming component of a site's velocity is determined at the centre of mass of the molecule, as opposed to the streaming-velocity at the site. For PCF these equations are,

$$\dot{\mathbf{r}}_{i\alpha} = \frac{\mathbf{p}_{i\alpha}}{m_{i\alpha}} + r_{yi}\hat{\mathbf{n}}_x\dot{\gamma}, \tag{9}$$

$$\dot{\mathbf{p}}_{i\alpha} = \mathbf{F}_{i\alpha}^{\mathrm{LJ}} + \mathbf{F}_{i\alpha}^{\mathrm{C/FENE}} - \frac{m_{i\alpha}}{M_i}\hat{\mathbf{n}}_x\dot{\gamma}p_{yi} - \zeta_{\mathrm{M}}\frac{m_{i\alpha}}{M_i}\mathbf{p}_i, \tag{10}$$

while for PEF the equations are,

$$\dot{\mathbf{r}}_{i\alpha} = \frac{\mathbf{p}_{i\alpha}}{m_{i\alpha}} + (r_{xi}\hat{\mathbf{n}}_x - r_{yi}\hat{\mathbf{n}}_y)\dot{\varepsilon}, \tag{11}$$

$$\dot{\mathbf{p}}_{i\alpha} = \mathbf{F}_{i\alpha}^{\mathrm{LJ}} + \mathbf{F}_{i\alpha}^{\mathrm{C/FENE}} - \frac{m_{i\alpha}}{M_i}(r_{xi}\hat{\mathbf{n}}_x - r_{yi}\hat{\mathbf{n}}_y)\dot{\varepsilon} - \zeta_{\mathrm{M}}\frac{m_{i\alpha}}{M_i}\mathbf{p}_i. \tag{12}$$

The combination of equations of motion and thermostat is collectively known as molecular SLLOD/molecular thermostat (MSMT). Our use of MSMT is the result of several investigations reported in the literature regarding the merits of different equations of motion and thermostats. For example, in the work of Padilla and Toxverd [43] it was shown that the results from atomic and molecular thermostated systems differed, but that results using the molecular thermostat were closer to those of a system which was thermostated by the surrounding fluid. Furthermore, in detailed investigations [19,20,44], it was found that the use of atomic SLLOD together with an atomic thermostat for molecular fluids led to an antisymmetric component in the molecular pressure tensor which imposed a torque on molecules as well as leading to excessive molecular alignment in the system. In contrast, it was found that this effect did not occur with the use of MSMT. One disadvantage of MSMT, especially for large molecules, is that the thermostat only acts on a fraction of the degrees of freedom in the system. At high strain-rates this may result in the degrees of freedom that are not thermostated to overheat. One way to avoid this is to use the newly devised configurational thermostat, such as that developed by Braga and Travis [45] and references therein, but for the purposes of our study, and the relatively moderate strain rates investigated, a molecular thermostat suffices.

2.3 Pressure tensor and energy

The pressure in a molecular liquid can be calculated using either of two expressions: the molecular or atomic pressure [17,19,42]. The molecular pressure is the pressure calculated using the intermolecular forces and the molecular centre of mass momenta. The instantaneous

expression for the molecular pressure is,

$$P_M V = \sum_{i=1}^{N_m} \frac{\mathbf{p}_i \mathbf{p}_i}{M_i} - \frac{1}{2} \sum_{i=1}^{N_m} \sum_{\alpha=1}^{N_s} \sum_{j \neq i}^{N_m} \sum_{\beta=1}^{N_s} \mathbf{r}_{ij} \mathbf{F}_{i\alpha j\beta}^{\text{inter}} \quad (13)$$

where $\mathbf{r}_{ij}$ is the minimum image separation of the centres of mass of molecules, $\mathbf{F}_{i\alpha j\beta}^{\text{inter}}$ is the interatomic force between site α on molecule i and site β on molecule j, $\mathbf{p}_i$ is the momentum of the centre of mass of molecule i and V is the volume of the system. Note that, in this case the second term, the virial, does not contain any intramolecular terms.

The atomic pressure on the other hand includes all atomic momenta and all interatomic forces and constraint forces. The expression for the atomic pressure is,

$$\begin{aligned} P_A V = & \sum_{i=1}^{N_m} \sum_{\alpha=1}^{N_s} \frac{\mathbf{p}_{i\alpha} \mathbf{p}_{i\alpha}}{m_{i\alpha}} \\ & - \frac{1}{2} \sum_{i=1}^{N_m} \sum_{\alpha=1}^{N_s} \sum_{j \neq i}^{N_m} \sum_{\beta=1}^{N_s} \mathbf{r}_{i\alpha j\beta} \mathbf{F}_{i\alpha j\beta} \\ & - \sum_{i=1}^{N_m} \sum_{\alpha=1}^{N_s - 1} \sum_{\beta > \alpha}^{N_s} \mathbf{r}_{i\alpha j\beta} \mathbf{F}_{i\alpha j\beta} + \sum_{i=1}^{N_m} \sum_{\alpha=1}^{N_s} \mathbf{r}_{i\alpha} \mathbf{F}_{i\alpha}^{C}. \end{aligned} \quad (14)$$

Here, $\mathbf{r}_{i\alpha j\beta}$ is the vector between atom α on molecule i and atom β on molecule j, $\mathbf{F}_{i\alpha j\beta}$ is the corresponding interatomic force between these atoms.

As already noted above, Travis et al. [19,20,44] have investigated the differences between results using the molecular and atomic SLLOD algorithms under PCF. Included in these investigations was a comparison of molecular and atomic pressure tensors. The instantaneous atomic pressure tensor is symmetric since the forces involved act between centres of atoms. In the case of the instantaneous molecular pressure tensor the virial term is the dyadic product of the vector between the centres of mass of two molecules and the forces between atoms in the molecules. This is in general not a central force and gives rise to an antisymmetric component of the instantaneous pressure tensor. However, it was found that the steady-state averages of both the atomic and molecular stress tensors agreed, confirming the results of Edberg et al. [17]. From the steady state averages of the pressure tensor prediction of the viscosities and normal stresses can be calculated. In the results that follow we include only molecular pressure tensor calculations.

The instantaneous total internal energy of the system is given by,

$$\begin{aligned} U = \frac{1}{N_m} \Bigg(& \sum_{i=1}^{N_m} \sum_{\alpha=1}^{N_s} \frac{\mathbf{p}_{i\alpha}^2}{2m_{i\alpha}} + \sum_{i=1}^{N_m - 1} \sum_{\alpha=1}^{N_s} \sum_{j=i+1}^{N_m} \sum_{\beta=1}^{N_s} U_{i\alpha j\beta} \\ & + \sum_{i=1}^{N_m} \sum_{\alpha=1}^{N_s - 2} \sum_{\beta=\alpha+2}^{N_s} U_{i\alpha j\beta} \Bigg). \end{aligned} \quad (15)$$

In this expression the total energy of the system has been separated into its kinetic, intermolecular and intramolecular components. $U_{i\alpha j\beta}$ is the potential energy between atom α on molecule i and atom β on molecule j. As in the case of the pressure tensor, we compute steady-state averages of the instantaneous values.

3. Simulation details

We have compared the results from simulations of 2,4,10,20 and 50-site monodisperse systems of FENE and FJC molecules under both PCF and PEF. We have also simulated 100-site FENE molecules under both flows. The number of molecules in each system and the range of strain rates simulated, is presented in Table 1. The simulations were performed using the molecular SLLOD algorithm [2,17,42], the Lees-Edwards PBCs [46] for PCF and the Kraynik-Reinelt PBCs for PEF [13–16], as previously noted. The equations of motion were integrated using a fourth order Gear predictor–corrector algorithm [47,48] with a reduced time step of $\Delta t = 0.001$ for all systems. To improve the efficiency of the force calculation, a neighbour list algorithm was used as well as a cell method. These algorithms are described for PCF by Allen and Tildesly [47] and for PEF by Matin et al. [6].

Data presented in this work were collected from simulations run at the reduced molecular temperature $T = 1.0$ and bead number density $\rho = 0.84$. Systems were initialised at a low density with beads on an FCC lattice. The systems were allowed to relax away from the lattice at this low density and were then compressed using a bulk

Table 1. Some details of systems simulated. N_s and N_m are the number of sites per molecule and number of molecules respectively, while II_{min} and II_{max} are the minimum and maximum strain rates, expressed as the second scalar invariant of the strain rate tensor, respectively.

N_s	N_m	II_{min}	II_{max}
2	500	1×10^{-4}	5.12
4	500	1×10^{-4}	5.12
10	500	1×10^{-5}	1.0
20	500	1×10^{-6}	5×10^{-1}
50	256	1×10^{-7}	5×10^{-2}
100	108	1×10^{-7}	1×10^{-3}

compression algorithm [1]. For some systems it was necessary to perform further equilibration at an intermediate density before compressing the system to the target density, at which the remainder of the simulations were performed.

We initially performed simulations of the FENE molecules so that we could obtain a comparable bond length for the subsequent simulations of the FJC molecules. The bond length that we chose was $b = 0.97$. Further details of this calculation can be found in Section 4.

For 2,4,10,20 and 50-site molecules each system was equilibrated at a set strain-rate for between 3.2×10^6 and 6.4×10^6 time-steps to ensure that the system had reached a steady state. For 100-site molecules this equilibration was extended to 4×10^7 time-steps. For the data that we present in this paper the results were calculated in the following way: every 25 time-steps the instantaneous value of a property was calculated; every 100 time-steps the average of the previous four values was printed to a file; after 4×10^5 time-steps this series was divided into 10 blocks and a block average, a total average and a standard error (SE) were calculated. In the case of 2,4,10,20 and 50-site systems, to further improve the statistics, the results of four consecutive simulations were averaged and a SE calculated, this gave the final results which are presented here. For 100-site systems, an average and SE were calculated from 100 consecutive simulations. The length of the simulations was also governed by requirements of the calculation of diffusion coefficients, which will be discussed in a separate paper.

Results are presented in terms of reduced units i.e. in terms of LJ coefficients ε_{LJ}, σ_{LJ} and the mass of a bead m; temperature is measured in terms of units k_B/ε_{LJ}. The conversion from real units to reduced units gives: the reduced density $\rho^* = \rho/\sigma_{LJ}^3$, the reduced temperature $T^* = k_B T/\varepsilon_{LJ}$, reduced time $t^* = \left(\varepsilon_{LJ}/m\sigma_{LJ}^2\right)^{1/2} t$, reduced pressure $p^* = p\sigma_{LJ}^3/\varepsilon_{LJ}$, reduced strain-rate $\dot{\gamma}* = \left(m\sigma_{LJ}^2/\varepsilon_{LJ}\right)^{1/2}\dot{\gamma}$, reduced viscosity $\eta^* = \left(\sigma_{LJ}^4/m\varepsilon_{LJ}\right)^{1/2}\eta$. For the remainder of the paper the asterisk is dropped. In our simulations we set $\varepsilon_{LJ} = \sigma_{LJ} = m = 1.0$. This choice of units is convenient for simulations because length and time scales are within a numerically manageable range [47].

4. Bond length calculation

The FENE potential allows the bond length between adjacent sites along the molecule to fluctuate. Thus, to perform a comparison between the FENE and FJC molecules we need to choose a suitable bond length for the FJC molecules.

After simulation of the FENE systems we calculated the mean and variance of bond lengths within the final configurations for each system. The number of bonds in the system ranged from 500 for the 2-site systems to 12,544 for the 50-site systems. Data from these calculations are given in the PhD thesis by Hunt [39] but not plotted here for brevity. We find that as the strain rate is increased the mean bond length increases only slightly for the shorter molecules. However, for the 50-site and 100-site molecules in PEF we find considerable stretching. The variance seen in the FENE bond length is not present in the FJC molecules, which is the main distinction between the two molecules. From these data we obtained a mean bond length over all systems of $\bar{b} = 0.970(8)$. This average value can be compared with the minimum of the bonding potential $b_{min} = 0.9608$, shown in Figure 1. If the assumption is made that the only potential in the system is this bonding potential, then we find numerically that the Boltzmann distribution

$$\mathrm{Prob}(b) \propto 4\pi b^2 \exp(-(U_{WCA}(b) + U_{FENE}(b))/k_B T), \quad (16)$$

gives an average bond length of $b_B = 0.9701$ and a standard deviation (SD) $\Delta b_B = 0.0334$. This value does not include intramolecular contributions from non-bonded sites, nor does it include any intermolecular interactions. We note that variance of the bond length is skewed above the mean with little deviation below $b = 0.93$. This is due to the steep repulsive potential during contraction of the bond.

Previous investigations of FJC systems [5,6,8,9] used a value of $b_{FJC} = 1.0$. This value is approximately one SD greater than the value we compute in our FENE systems with $\mathrm{II} < 10^{-4}$, where II is defined as the second scalar *in*variant of the strain rate tensor and takes on the values of $\mathrm{II} = 2\dot{\gamma}^2$ for PCF and $8\dot{\varepsilon}^2$ for PEF. This variable is proportional to the rate of viscous heat dissipation in the system at steady state and therefore we are more easily able to compare systems under different flow which are in a similar non-equilibrium state. Though we could have chosen an individual FJC bond length for each strain rate, for convenience we have used just the single value of $b_{FJC} = 0.97$ corresponding to the mean value of the FENE bond length.

5. Results

5.1 *Rheological properties*

In this section we compare the rheological properties of the FENE and FJC molecules. These are properties which are directly derived from the stress tensor. We include the shear and extensional viscosities η and $\bar{\eta}$ and the various normal stresses.

5.1.1 *Extensional and shear viscosity*

We have calculated the steady state shear and extensional viscosities for both FENE and FJC molecules. These

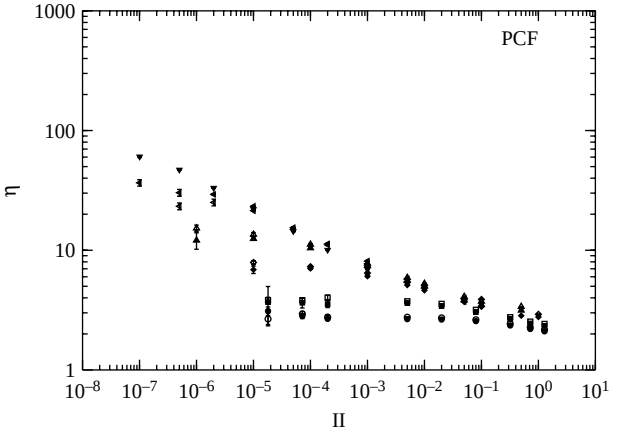

Figure 2. Comparison of the shear viscosity η for FJC molecules (open symbols) and FENE molecules (closed symbols). The symbols correspond to 2-site systems (circles), 4-site systems (squares), 10-site systems (diamonds), 20-site systems (triangles-up), 50-site systems (triangles-left) and 100-site systems (triangles-down).

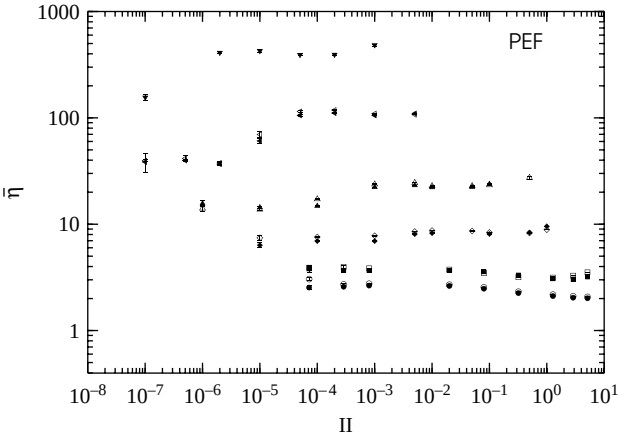

Figure 3. Comparison of the extensional viscosity $\bar{\eta}$ for FJC and FENE molecules of length 2,4,10,20 and 50 monomers. We have included just FENE molecules for the 100-site systems. The symbols are the same as in Figure 2.

functions are given in terms of the pressure tensor by

$$\eta = \frac{P_{xy} + P_{yx}}{2\dot{\gamma}}$$

and

$$\bar{\eta} = \frac{P_{yy} - P_{xx}}{4\dot{\varepsilon}}$$

for PCF and PEF respectively and are plotted against the second scalar invariant II in Figures 2 and 3. From the data presented in the two figures we see that the viscosities of the FENE and FJC molecules are very similar. In Figure 3 we see for longer molecules the characteristic increase and plateau in $\bar{\eta}$. For simulations at constant volume the viscosity then begins to increase again. However, Daivis et al. [8] have found that if the simulations are performed with constant P_{zz} then the viscosity decreased after the plateau. The shear viscosity for longer molecules (Figure 2) shows that in PCF shear-thinning occurs independent of the molecular weight.

As the strain-rate decreases the systems approach the zero strain-rate viscosity. To estimate the zero strain-rate viscosities for the two molecules we have performed least-squares fits to the viscosity. The functional forms that we used for this were, $y = A + Bx$, $y = A + Bx^2$ and $y = A + Bx^{1/2}$, where the pair (x, y) is $(\dot{\gamma}, \eta)$ and $(\dot{\varepsilon}, \bar{\eta})$ for PCF and PEF, respectively. The parameter A corresponds to the zero strain-rate viscosity. For each system and functional form we used four to eight data points of lowest strain-rate and chose the fit which gave the highest regression coefficient. We then averaged the zero strain-rate viscosity (A) to give the estimates of η_0 and $\bar{\eta}_0$ presented in Table 2. We see from this data that for the shorter molecules under PCF and PEF the viscosity of the FJC system is larger than

Table 2. Comparison of the zero strain-rate viscosities η_0 and $\bar{\eta}_0$ for FENE and FJC molecules extrapolated from the finite strain-rate viscosities.

Flow	PCF		PEF	
Molecule	FENE η_0	FJC η_0	FENE $\bar{\eta}_0$	FJC $\bar{\eta}_0$
2-Site	2.79(4)	2.86(4)	2.81(3)	2.87(5)
4-Site	3.83(1)	4.02(7)	3.82(4)	3.99(4)
10-Site	6.1(1)	7.6(2)	6.5(2)	7.2(2)
20-Site	12.4(2)	13.6(3)	12.2(3)	12.8(3)
50-Site	37.2(5)	30.9(4)	29.8(5)	33.3(4)
100-Site	50(10)	–	160(10)	–
10 to 50-Sites	$0.54(5)N^{1.09(3)}$	$1.2(1)N^{0.84(3)}$	$0.88(8)N^{0.90(5)}$	$0.94(7)N^{0.91(5)}$
10 to 100-Sites	$0.54(4)N^{1.09(3)}$	–	$0.73(6)N^{0.97(5)}$	–

The last two rows give the least-squares fit parameters for η_0, $(\bar{\eta}_0) = \mu N^{\nu}$ using the 10-site to 50-site data and 10-site to 100-site data ($N = N_S - 1$).

the viscosity of the FENE system. Under PEF this trend is observed for all chain lengths studied here. Including data for all flows, the difference between the viscosities for FENE and FJC molecules as a percentage of their average value varies between 3% for 2-site molecules under PCF and 22% for 10-site molecules under PCF; there is no clear trend in the overall variation with molecular weight. For 100-site systems we have estimated $\bar{\eta}_0$ with the extensional viscosity at $\mathrm{II} = 1 \times 10^{-7}$. This probably gives an over-estimate of $\bar{\eta}_0$ for 100-site molecules.

In Figure 4 we have plotted the zero strain-rate viscosity against the length of the molecule N_s. It is well known [25,49] that this data should follow the relationship

$$\eta_0 = \mu N^{\nu}, \quad \bar{\eta}_0 = \mu N^{\nu}, \tag{17}$$

where $N = N_s - 1$ is the number of bonds in the molecule. The parameters of the least-squares fit to the viscosity data for 10 to 50-site molecules is given in the second last row of Table 2 and the fit to data for 10 to 100-site molecules is given in the last row of Table 2. The average of the exponent over all systems for the range 10 to 50-site is $\nu = 0.93(9)$. The best fit for PCF data with systems in the range 10 to 100-site gives the exponent $\nu = 1.08(3)$. This is very close to the expected value $\nu = 1.0$ as predicted by the Rouse model and found by Kröger and Hess [25] in their simulations of FENE molecules. The greatest difference between FENE and FJC is seen in the exponent ν calculated for the range 10 to 50-site; the FJC systems having a smaller exponent ($\nu = 0.84(3)$) than the FENE molecules ($\nu = 1.09(3)$). It should be noted that a fit to systems in the range 2 to 50-site gives a much smaller exponent, $\nu \approx 0.77$. Two-site molecules do not exhibit Rouse behaviour and thus the inclusion of these molecules in the calculation of ν leads to its decreased value.

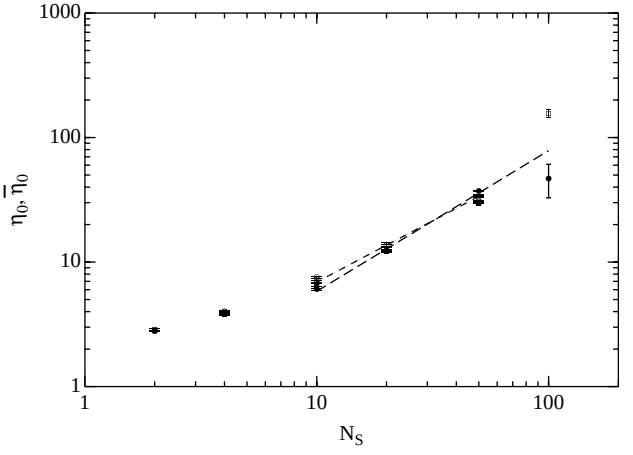

Figure 4. Comparison of the zero strain-rate viscosity for PCF (circles) and PEF (squares). Open symbols correspond to FJC molecules, closed symbols correspond to FENE molecules. The dashed line (– -) is the best fit to the 10-site to 100-site PCF data ($\eta_0 = 0.87(N_s - 1)^{0.93}$). The dot-dashed line (-.-.) is the best fit to the 10-site to 50-site data averaged over all systems ($\eta_0 = 0.54(N_s - 1)^{1.08}$).

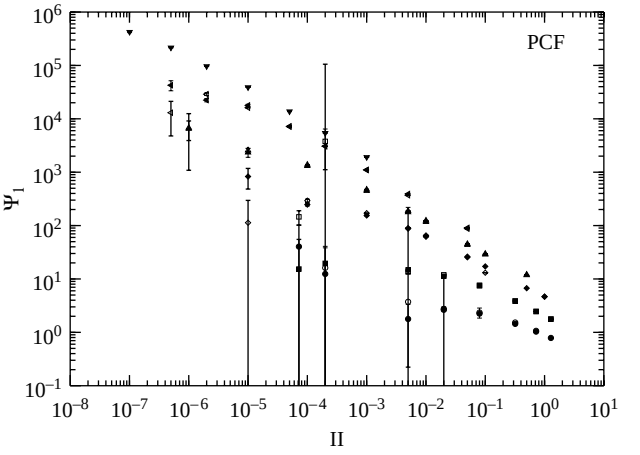

Figure 5. First normal stress Ψ_1 for FJC and FENE molecules of length 2,4,10,20 and 50 monomers. We include data for 100-site FENE molecules. The system is under shear flow (PCF). The symbols are the same as in Figure 2.

5.1.2 *Normal stress differences*

Data for the steady state first (Ψ_1) and second (Ψ_2) normal stress coefficients under PCF are presented in Figures 5 and 6, respectively. These are defined as,

$$\Psi_1 = \frac{P_{yy} - P_{xx}}{\dot{\gamma}^2},$$

$$\Psi_2 = \frac{P_{zz} - P_{yy}}{\dot{\gamma}^2}.$$

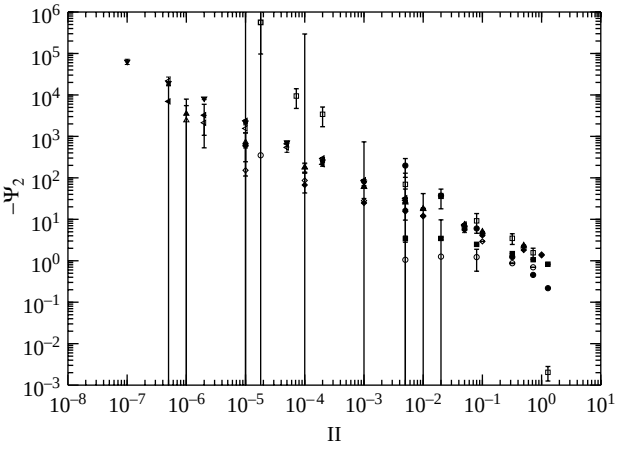

Figure 6. Second normal stress $-\Psi_2$ for FJC and FENE molecules of length 2,4,10,20 and 50 monomers. We include data for 100-site FENE molecules. The system is under shear flow (PCF). The symbols are the same as in Figure 2.

Normal stress coefficients measure the difference between stresses normal to the faces of a cubic volume of fluid. It had been suggested (the Weissenberg Hypothesis [22,50]) that the second normal stress in fluids is zero, however it is now known that Ψ_2 is about 10% of the value of Ψ_1. From the simulation data it is seen that both functions decrease in value as the strain-rate is increased. In general, these functions show an increase with molecular length, which is comparable with viscosity. However, in comparison with the shear viscosity, the range of Ψ_1 is about an order of magnitude greater, particularly for longer molecules. The statistical variance in this data is considerable, especially for Ψ_2. The ratio $-\Psi_1/\Psi_2$ has a large variance as a consequence of the variance in both terms [39]. From this data we can only estimate the ratio at being between 0.1 and 1.0 for most systems. The difference between the data for FENE and FJC is also greatest for these quantities. However, without better statistics we are unable to make any stronger conclusions about this difference.

Under extensional flows, the first and second extensional viscosities are

$$\eta_1 = \frac{P_{yy} - P_{xx}}{\dot{\varepsilon}}$$

and

$$\eta_2 = \frac{P_{yy} - P_{zz}}{\dot{\varepsilon}},$$

respectively. The first extensional viscosity η_1 is proportional to the extensional viscosity ($4\bar{\eta} = \eta_1$) and therefore we do not discuss it further here. Data for the second extensional viscosity η_2 is presented in Figure 7. Daivis et al. [8] note that this function has been measured only rarely and cite just Wagner et al. [51] who measure the transient value of this function. Comparing with other viscometric functions for PEF and PCF we note that there is less variation with molecular weight for this function. η_2 decreases and then has a small region of increase at large strain rates. As for the viscosity, this increase did not occur when simulations were performed with constant P_{zz} by Daivis et al. [8]. The ratio η_2/η_1 has better statistics than the normal stress coefficients for PCF [39] and approaches the value $1/2$ for low strain-rates, but has a larger value for short molecules. Matin [7] explains this property by noting that in the Newtonian regime, P_{zz} does not change and the positive change in P_{yy} is equal in magnitude to the negative change in P_{xx}. It is seen from this ratio that for larger molecules η_1 dominates η_2 and there is a region over which the ratio is approximately constant. In each of the functions described here there is little variation between the values for FENE and FJC molecules.

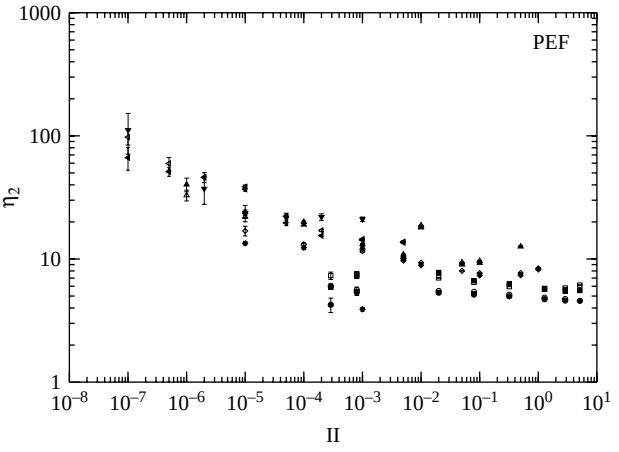

Figure 7. Second normal stress η_2 for FJC and FENE molecules of length 2,4,10,20 and 50 monomers. We include data for 100-site FENE molecules. The system is under extensional flow (PEF). The symbols are the same as in Figure 2.

5.2 *Microscopic properties*

An important feature of molecular simulations is the accessibility of the molecular details of a system, which allows the direct calculation of microscopic properties which in experiment would require sophisticated optical or scattering techniques. In this section, we investigate the alignment and extension of molecules in flow, as well as their rotation. Similar calculations of the FJC molecule with $b = 1.0$ under PEF and PCF have been performed by Matin et al. [5] for small molecules up to four sites in length. Calculations for dendrimer and linear FENE molecules under PCF at $T = 1.25$ have also been presented by Bosko et al. [26,31,32].

5.2.1 *Extension of molecules*

At equilibrium it is known that the orientation of molecules in a melt is isotropic. However, away from equilibrium, under flow, it is well known that molecules align, i.e. Maxwell's effect or flow birefringence. In this section and the next we introduce several measures which give a quantitative indication of the change in conformation of molecules in the system.

For an individual molecule composed of identical particles the tensor of gyration is given by,

$$\mathrm{R}_g^2 \equiv \frac{1}{2N_s^2} \sum_{\alpha,\beta=1}^{N_s} (\mathbf{r}_\alpha - \mathbf{r}_\beta)^2 \qquad (18)$$

where $\mathbf{r}_\alpha$ and $\mathbf{r}_\beta$ are the positions of beads α and β, respectively. The radius of gyration is defined as $R_g^2 = \mathrm{trace}\left(\mathrm{R}_g^2\right)$ and is proportional to the scalar moment of inertia $I_m = MR_g^2$, where M is the total mass of the molecule. In the case here where each of the beads has

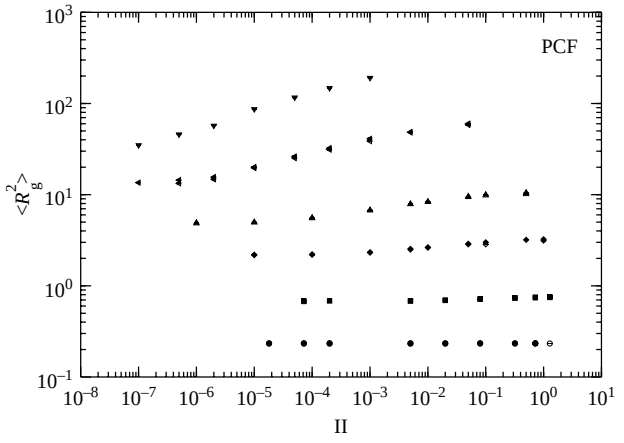

Figure 8. Comparison of the mean-squared radius of gyration $\langle R_g^2 \rangle$ for FJC and FENE molecules of length 2,4,10,20 and 50 monomers. We include data for 100-site FENE molecules. The system is under shear flow (PCF). The symbols are the same as in Figure 2.

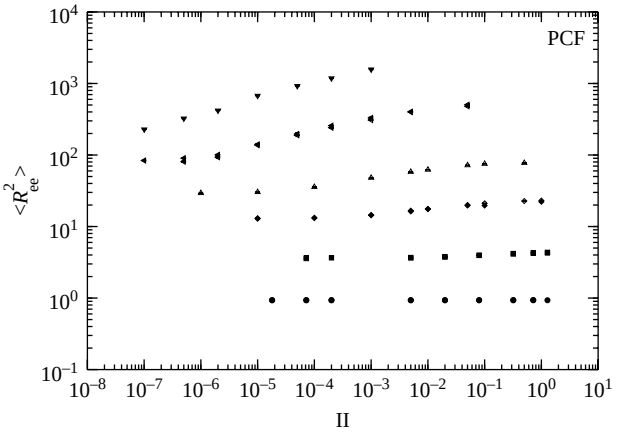

Figure 10. Comparison of the mean-squared end-to-end distance $\langle R_{ee}^2 \rangle$ for FJC and FENE molecules of length 2,4,10,20 and 50 monomers. We include data for 100-site FENE molecules. The system is under shear flow (PCF). The symbols are the same as in Figure 2.

the same mass, the moment of inertia *tensor* is -1 times the traceless part of R_g^2. The gyration tensor was averaged over all molecules in the system and the average radius of gyration squared $\left(\langle R_g^2 \rangle\right)$ calculated. Results of $\langle R_g^2 \rangle$ are presented in Figure 8 for PCF and in Figure 9 for PEF.

A further indication of the structure within the liquid is provided by calculation of the average mean-squared end-to-end distance $\langle R_{ee}^2 \rangle$ of molecules. This has again been calculated as an average over the molecules in the system and then as a time average. Results for PCF and PEF are presented in Figures 10 and 11, respectively.

For the smallest molecules, 2 and 4-site, there is little variation in $\langle R_g^2 \rangle$ and $\langle R_{ee}^2 \rangle$ for all systems. For the 2-site FJC molecules it is clear that these quantities are necessarily fixed. For the longer molecules (10 to 100-sites) it is seen that both $\langle R_{ee}^2 \rangle$ and $\langle R_g^2 \rangle$ increase with the strain-rate except at the highest strain-rate for PEF, where there is seen to be a slight decrease in these functions. This is attributed to the use of the constant volume algorithm rather than constant pressure algorithm. The plateau value of $\langle R_{ee}^2 \rangle$, at high strain-rates, indicates that under PEF molecules become fully extended. For example, in the case of 50-site molecules, the full extension of a molecule would correspond to $R_{ee}^2 = (49 \times 0.97)^2 = 2259$ which is close to the observed plateau value. As was the case for the rheological properties, there is almost no variation between FENE and FJC molecules for these structural properties. The

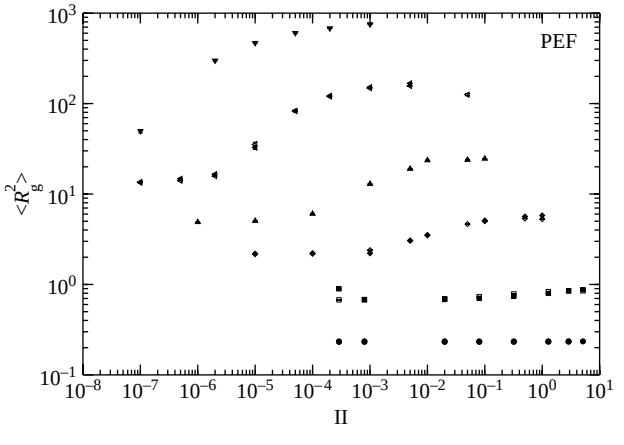

Figure 9. Comparison of the mean-squared radius of gyration $\langle R_g^2 \rangle$ for FJC and FENE molecules of length 2,4,10,20 and 50 monomers. We include data for 100-site FENE molecules. The system is under extensional flow (PEF). The symbols are the same as in Figure 2.

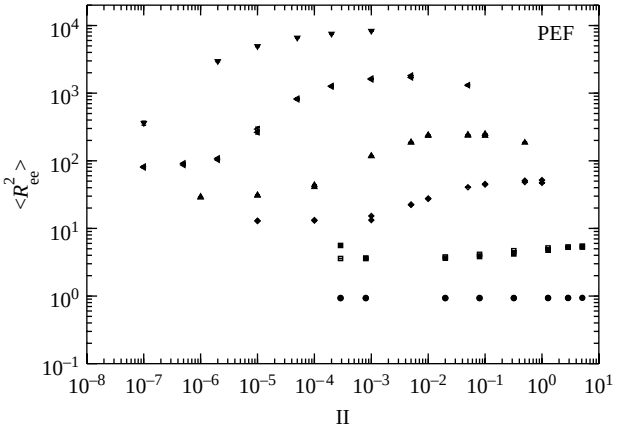

Figure 11. Comparison of the mean-squared end-to-end distance $\langle R_{ee}^2 \rangle$ for FJC and FENE molecules of length 2,4,10,20 and 50 monomers. We include data for 100-site FENE molecules. The system is under extensional flow (PEF). The symbols are the same as in Figure 2.

observed variation in the FENE bond length, presented above, has little effect since, instantaneously, some bonds will be longer and others shorter.

5.2.2 *The order tensor*

From the gyration tensor we are able to obtain more details about the alignment in the systems. We have calculated the order tensor **S**, which is a symmetric traceless tensor calculated instantaneously during a simulation using the relation,

$$\mathbf{S} = \frac{1}{N_{\mathrm{m}}} \sum_{i=1}^{N_{\mathrm{m}}} \left(\hat{\mathbf{u}}_i \hat{\mathbf{u}}_i - \frac{1}{3}\mathbf{I} \right), \tag{19}$$

where $\hat{\mathbf{u}}_i$ is the unit vector corresponding to the largest eigenvalue of the gyration tensor for molecule i and **I** is the isotropic tensor. This tensor represents a collection of correlation coefficients; each element $S_{\alpha\beta}$ is the correlation between the component $u_{i\alpha}$ and $u_{i\beta}$ of the unit vector for an individual chain.

From the order tensor one can obtain the order parameter S, which is a single numerical indicator of the alignment in a system. The order parameter is $3/2$ of the largest eigenvalue of the tensor **S**, and the corresponding eigenvector is the direction of alignment in the system. The value of S has the range $0 \leq S \leq 1$. When $S = 0$ the molecules are isotropic while when $S = 1$ the molecules are perfectly aligned.

The order parameter for systems under PCF and PEF is presented in Figures 12 and 13, respectively. It is seen from both figures that, in general, S increases with the increase of the strain-rate. However, there is a distinction between the alignment for PCF and PEF: while for PEF, the order parameter reaches a plateau value and remains at this value over a wide range of strain rates, for PCF a plateau is only reached at very high strain-rates and only for longer molecules. It is also seen that for larger molecules the increase in alignment begins at a lower strain-rate and occurs more rapidly. Qualitatively this is similar to the earlier onset of non-Newtonian behaviour for longer molecules. The alignment shows little difference between FENE and FJC systems, however, under PEF in the range where S increases there is greatest variation between the two molecules. The sensitivity on strain-rate in this region would suggest that the uncertainty in these values is greater. For PEF there is also a slight decrease in S at the highest strain-rates, which again corresponds to rates where the difference between the constant volume and constant pressure algorithms has been observed by Daivis et al. [8].

5.2.3 *Alignment angle*

From the order tensor one can also calculate the alignment angle (also known as the birefringence extinction angle).

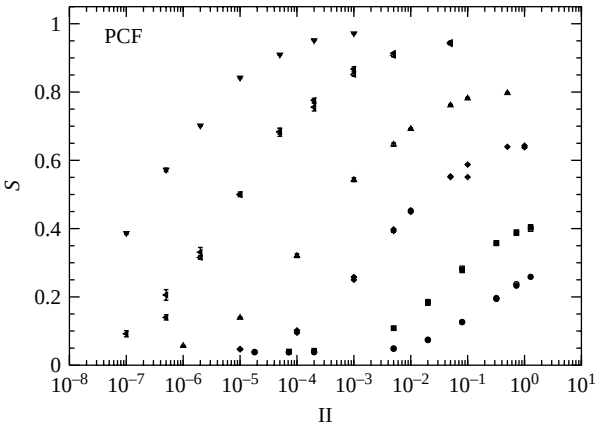

Figure 12. Comparison of the order parameter S for FJC and FENE molecules of length 2,4,10,20 and 50 monomers. We include data for 100-site FENE molecules. The system is under shear flow (PCF). The symbols are the same as in Figure 2.

This is the angle χ that a molecule makes on average with the x-axis in the xy-plane. If the largest eigenvector of the gyration tensor of a molecule is $\hat{\mathbf{e}} = (e_x, e_y, e_z)$ then in planar flows the z component vanishes ($e_z = 0$) because there is on average no component of alignment in the $\hat{\mathbf{n}}_z$ direction. For this situation we have,

$$\chi = \arctan\left(\frac{e_y}{e_x}\right). \tag{20}$$

While for PEF it is known [7] that the alignment is parallel with the x-axis, for PCF in the Newtonian regime molecules align on average with $\chi = 45°$. Results for χ under PCF are presented in Figure 14 and it is seen that in the non-Newtonian regime the alignment angle decreases

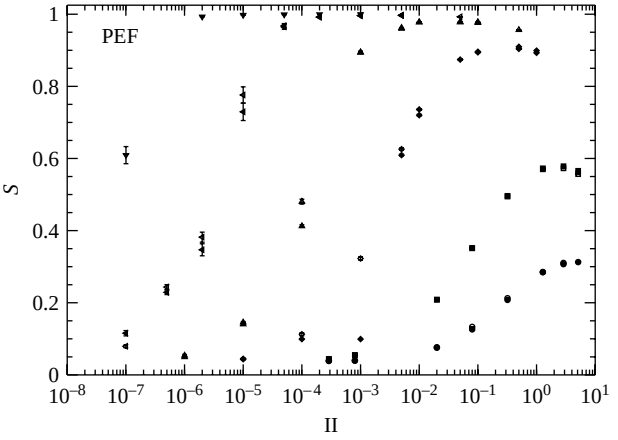

Figure 13. Comparison of the order parameter S for FJC and FENE molecules of length 2,4,10,20 and 50 monomers. We include data for 100-site FENE molecules. The system is under extensional flow (PEF). The symbols are the same as in Figure 2.

with the strain-rate. At a single strain-rate, χ decreases with the molecular length, which is due to the earlier onset of the non-Newtonian regime for longer molecules. It is not explicitly clear from this data that molecules approach the 45° alignment in the Newtonian regime. 100-site molecules only reach $\chi = 20°$ at the lowest strain rate we have considered, 50-site molecules do approach $\chi = 40°$, however, the FENE result for the lowest strain rate has an alignment of approximately $\chi = 55°$. For shorter molecules –2, 4 and 10-sites – there is a strain-rate below which χ diverges significantly from the trend towards alignment at $\chi = 45°$. Comparing with the order parameter in Figure 12 it is clear that at these low strain-rates there is less ordering in the fluid and so longer simulation times are required to obtain a better estimate for the average alignment angle. Furthermore, for larger molecular weights one needs to perform simulations at even weaker strain-rates than we have done to obtain the limiting $\chi = 45°$ behaviour. It is seen once more that there is little difference between FENE and FJC molecules.

5.2.4 *Spin angular velocity*

Despite the alignment of molecules which has been described and calculated in the preceding sections, molecules also undergo rotation in PCF; under PEF it has been found that the average angular momentum for molecules is zero [5,7]. For PCF it is found that in the Newtonian regime the spin angular velocity of molecules should be $\dot{\gamma}/2$ in the clockwise sense about the $\hat{\mathbf{n}}_z$ direction [21]. The instantaneous angular velocity of molecules is calculated by inverting the relation,

$$\mathbf{L} = \mathrm{I_m} \cdot \boldsymbol{\omega}, \tag{21}$$

where $\mathbf{L}$ is the angular momentum of the molecule with respect to its centre of mass, $\mathrm{I_m}$ is the moment of inertia tensor and $\boldsymbol{\omega}$ is the angular velocity vector. Once calculated, the components of the instantaneous angular velocity are averaged over the course of a simulation, in a similar way to the preceding properties.

We have confirmed that for PEF all components of the angular velocity are on average zero. Under PCF just the component ω_z is non-zero and values for this component are shown in Figure 15. The line $-\dot{\gamma}/2$ is also plotted in this figure. It is seen that for 4 to 50-site molecules the angular velocity approaches $-\dot{\gamma}/2$ at low strain-rates. This is a relationship which is predicted by irreversible thermodynamics [21,52] in the steady-state and the limit as $\dot{\gamma} \to 0$. We have not simulated the 100-site system at small enough strain-rates to confirm this behaviour for this system and the uncertainties in data for the 2-site system were too large for this data to be included. Considering data in the non-Newtonian regime, we see that on a log-log plot ω_z has a linear relationship to $\dot{\gamma}$ which would suggest a power-law $\omega_z = \alpha\dot{\gamma}^{\beta}$. Coefficients for this relationship are presented in Table 3. The coefficient β is seen to decrease with larger molecular weight, i.e. at equal strain-rates, the increase of molecular weight results in a decreased propensity for the molecules to rotate. This can be explained by the increased hindrance from surrounding molecules. Note that, the systems we consider only approach the entanglement regime for 100-site molecules.

There is again little difference between the results for FENE and FJC molecules. The greatest difference is in the 50-site data where the error bars are much larger for FENE molecules. This would indicate that there is more variation in the angular velocity of FENE molecules than FJC molecules, however, it is unclear whether this is an artefact of the averaging process.

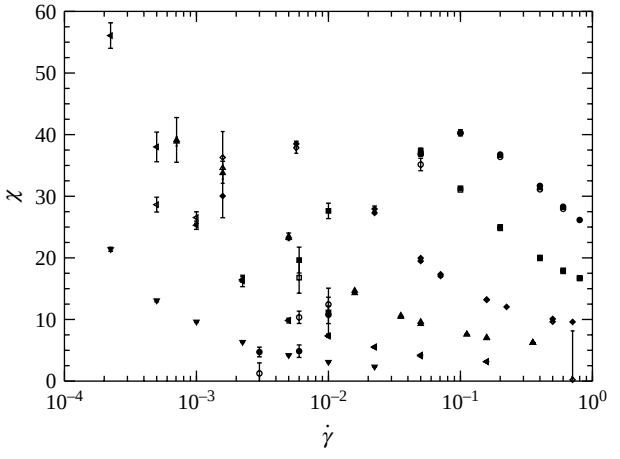

Figure 14. The alignment angle χ under PCF. Symbols are the same as in Figure 2. A($\dot{\gamma}/2$).

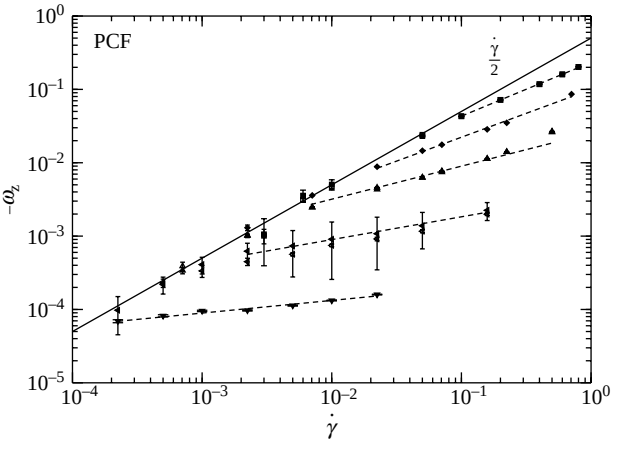

Figure 15. The z component ω_z of the average spin angular velocity of molecules for systems under PCF. The line $\omega_z = \dot{\gamma}/2$ has been plotted for comparison in the Newtonian regime. The symbols are the same as in Figure 2. A least-squares fit (dashed lines) to a power law $\omega_z = \alpha\dot{\gamma}^{\beta}$ is also shown for each molecular weight.

Table 3. Results for the least-squares fit to ω_z in the power-law region for systems under PCF.

Molecule	α	β ($\omega_z = \alpha\dot{\gamma}^{\beta}$)
4-Site FENE	0.733	2.34×10^{-1}
4-Site FJC	0.743	2.37×10^{-1}
10-Site FENE	0.648	9.96×10^{-2}
20-Site FENE	0.552	3.41×10^{-2}
20-Site FJC	0.575	3.55×10^{-2}
50-Site FENE	0.311	3.75×10^{-3}
50-Site FJC	0.339	3.46×10^{-3}
100-Site FENE	0.170	2.91×10^{-4}

The simulation results together with these functions are presented in Figure 15.

5.2.5 *Algorithm efficiency*

It is well known that the calculation of forces is the most computationally expensive part of molecular dynamics simulations [47]. For this reason it is useful to compare the efficiency of the FENE and FJC force calculations. Within the force calculation the most intensive part is the calculation of interatomic distances. In our simulations this part of the calculation has been accelerated with the use of both neighbour-list and cell method algorithms. We do not discuss this aspect here, referring the reader to the work of Matin et al. [6]. We have estimated the relative efficiency of the FENE and FJC algorithms and present these details in Table 4. These estimates include just the calculation of the forces once the distance between atoms has been determined. It is seen that the FENE calculation represents only a small percentage of the full simulation and does not increase above 5% for the systems studied here. In contrast, the constraint calculation for FJC simulations is found to represent an increasing percentage of the simulation time. The efficiency of the constraint algorithm is limited by the linear algebra calculation involved [3]. The algorithm uses a *general* LU solver [53] which does not take into account the sparse nature of the constraint matrix. This deficiency has recently been investigated by Daivis and we are informed (Daivis P.J. private communication, 2007) that the efficiency of the constraint algorithm has been significantly improved by using sparse matrix solvers. All simulations were performed on the NEC TX7 supercomputer which has a vector parallel architecture.

6. Conclusion

We find that the structural properties of FENE and FJC molecules are on average almost identical over the wide range of strain and elongation rates studied. Given this, we can argue that the rheological properties for the two molecules should also be very similar in the steady state. Considering that the molecular pressure tensor involves only intermolecular forces and the centre of mass momenta, the contributions to this pressure tensor from the two molecules should be almost the same. In essence any potential between adjacent beads along the chain which give the same structure to a molecule will result in similar rheological properties in the steady state. This is indeed observed in our simulations, as demonstrated by the computed rheological properties for both molecular models.

Table 4. Comparison of the efficiency of the FENE and FJC algorithms.

Molecule	N_m	t_{FENE}/t_{total} (%)	t_{FJC}/t_{total} (%)	t_{FJC}/t_{FENE}
2-Site	500	1.9	2.0	1.0
4-Site	500	3.2	4.9	1.6
10-Site	500	3.5	32	11
20-Site	500	4.0	41	16
50-Site	256	4.1	68	43
100-Site	108	4.5	86	260

The times t_{FENE} and t_{FJC} included just force calculation after the distance between atoms has been determined. The time t_{total} used was the total CPU time of test simulations.

It has been shown [17] that for identical systems, the atomic pressure tensor gives the same result as the molecular pressure tensor in the steady state. However, the results of these functions under transient flows differ. Again we would expect that the use of the molecular pressure tensor in transient flows will give the same results for FENE and FJC molecules. However, if we used the atomic pressure tensor, we would expect there to be a difference between the molecules since the atomic pressure would include intramolecular forces in the calculation differentiating between FENE and FJC systems.

From our results we conclude that for the purposes of studying the molecular rheology of steady-state polymeric systems it is computationally more efficient to use the FENE molecular model over the FJC model, though we note that sparse matrix solvers in the case of the latter could narrow this efficiency gap somewhat. There does not seem to be any compelling evidence to support *a priori* use of the computationally more intensive FJC model, since all structural and rheological properties between both models are very similar in the steady-state. This is also true for diffusion of chains under either PCF or PEF, which will be presented in a subsequent publication. Finally, we point out that our work was conducted on chains without torsion constraints. In the case of semiflexible chains the FENE and FJC implementations could lead to significantly different results, depending on the degree of chain stiffness. Modifications to the FENE and bending potentials for such chains have been discussed by Kröger [54].

Acknowledgements

We thank Prof P.J. Daivis and Dr M.L. Matin for the use of their FJC code and also for many fruitful and stimulating discussions. We thank Dr A. Uhlherr and CSIRO Advanced Scientific Computing for generous provision of time on the NEC SX/TX supercomputers. BDT thanks Dr J.S. Hansen for assistance with latex typesetting.

Note

1. Email: tomahunt@gmail.com

References

[1] D.J. Evans and G.P. Morriss, *Statistical Mechanics of Non-equilibrium Liquids*, 2nd ed., Academic Press, New York, 1990.

[2] R. Edberg, D.J. Evans, and G.P. Morriss, *Constrained molecular dynamics: simulations of liquid alkanes with a new algorithm*, J. Chem. Phys. 84(12) (1986), pp. 6933–6939.

[3] G.P. Morriss and DJ Evans, *A constraint algorithm for the computer simulation of complex molecular liquids*, Comput. Phys. Commun. 62 (1991), pp. 267–278.

[4] J.K. Johnson, EA Muller, and K.E. Gubbins, *Equation of state for Lennard-Jones chains*, J. Phys. Chem. 98 (1994), pp. 6413–6419.

[5] M.L. Matin, P.J. Daivis, and B.D. Todd, *Comparison of planar shear flow and planar elongational flow for systems of small molecules*, J. Chem. Phys. 113(20) (2000), pp. 9122–9131.

[6] M. Matin, P.J. Daivis, and B.D. Todd, *Cell neighbour list method for planar elongational flow: rheology of a diatomic fluid*, Comput. Phys. Commun. 151 (2003), pp. 35–46.

[7] Matthew Leo Matin, *Molecular simulation of polymer rheology*, PhD thesis, Royal Melbourne Institute of Technology, 2001.

[8] P.J. Daivis, M.L. Matin, and B.D. Todd, *Nonlinear shear and elongational rheology of model polymer melts by non-equilibrium molecular dynamics*, J. Non-Newtonian Fluid Mech. 111 (2003), pp. 1–18.

[9] P.J. Daivis, M.L. Matin, and B.D. Todd, *Nonlinear shear and elongational rheology of model polymer melts at low strain rates*, J. Non-Newtonian Fluid Mech. 147(1–2) (2007), pp. 35–44.

[10] T. Kairn, P.J. Daivis, M.L. Matin, and I.K. Snook, *Concentration dependence of viscometric properties of model short chain polymer solutions*, Polymer 45 (2004), pp. 2453–2464.

[11] T. Kairn, P.J. Daivis, M.L. Matin, and I.K. Snook, *Effects of concentration on the steady-state viscometric properties of short chain polymer solutions over the entire concentration range*, Int. J. Thermophys. 25(4) (2004), pp. 1075–1084.

[12] T. Kairn, P.J. Daivis, I. Ivanov, and S.N. Bhattacharya, *Molecular-dynamics simulation of model polymer nanocomposite rheology and comparison with experiment*, J. Chem. Phys. 123 (2005), 194905.

[13] A.M. Kraynik and D.A. Reinelt, *Extensional motions of spatially periodic lattices*, Int. J. Multiphase Flow 18 (1992), p. 1045.

[14] B.D. Todd and P.J. Daivis, *Nonequilibrium molecular dynamics simulations of planar elongational flow with spatially and temporally periodic boundary conditions*, Phys. Rev. Lett. 81 (1998), p. 1118.

[15] B.D. Todd and P.J. Daivis, *A new algorithm for unrestricted duration molecular dynamics simulations of planar elongational flow*, Comput. Phys. Commun. 117 (1999), p. 191.

[16] B.D. Todd and P.J. Daivis, *The stability of nonequilibrium molecular dynamics simulations of elongational flows*, J. Chem. Phys. 112 (2000), p. 40.

[17] R. Edberg, G.P. Morriss, and D.J. Evans, *Rheology of* n*-alkanes by nonequilibrium molecular dynamics*, J. Chem. Phys. 86(8) (1987), pp. 4555–4570.

[18] M.N. Hounkonnou, C. Pierleoni, and J.P. Ryckaert, *Liquid chlorine in shear and elongational flows: a nonequilibrium molecular dynamics study*, J. Chem. Phys. 97(12) (1992), pp. 9335–9343.

[19] K.P. Travis, P.J. Daivis, and D.J. Evans, *Computer simulation algorithms for molecules undergoing planar Couette flow: a nonequilibrium molecular dynamics study*, J. Chem. Phys. 103(3) (1995), pp. 1109–1118.

[20] K.P. Travis, P.J. Daivis, and D.J. Evans, *Thermostats for molecular fluids undergoing shear flow: application to liquid chlorine*, J. Chem. Phys. 103 (1995), p. 10638.

[21] R. Edberg, D.J. Evans, and G.P. Morriss, *On the nonlinear Born effect*, Mol. Phys. 62(6) (1987), pp. 1357–1369.

[22] R. Byron Bird, R.C. Armstrong, and O. Hassager, *Dynamics of Polymeric Liquids, Volume 1: Fluid Mechanics*, 2nd ed., John Wiley and Sons, New York, 1987.

[23] M. Kröger, W. Loose, and S. Hess, *Rheology and structural changes of polymer melts via nonequilibrium molecular dynamics*, J. Rheol. 37 (1993), pp. 1057–1079.

[24] R. Muller, J.J. Pesce, and C. Picot, *Chain conformation in sheared polymer melts as revealed by SANS*, Macromolecules 26(16) (1993), pp. 4356–4362.

[25] M. Kröger and S. Hess, *Rheological evidence for a dynamical crossover in polymer melts via nonequilibrium molecular dynamics*, Phys. Rev. Lett. 85(5) (2000), pp. 1128–1131.

[26] J.T. Bosko, B.D. Todd, and R.J. Sadus, *Viscoelastic properties of dendrimers in the melt from nonequilibrium molecular dynamics*, J. Chem. Phys. 121(23) (2004), pp. 12050–12059.

[27] M. Kröger, C. Luap, and R. Muller, *Polymer melts under uniaxial elongational flow: stress-optical behaviour from experimental and nonequilibrium molecular dynamics computer simulations*, Macromolecules 30(3) (1997), pp. 526–539.

[28] C. Baig, B.J. Edwards, D.J. Keffer, H.D. Cochran, and V.A. Harmandaris, *Rheological and structural studies of linear polyethylene melts under planar elongational flow using non-equilibrium molecular dynamics simulations*, J. Chem. Phys. 124 (2006), 084902.

[29] J.M. Kim, D.J. Keffer, M. Kröger, and B.J. Edwards, *Rheological and entanglement characteristics of linear-chain polyethylene liquids in planar Couette and planar elongational flows*, J. Non-Newtonian Fluid Mech. 152 (2008), pp. 168–183.

[30] J.I. Siepmann, S. Karaboni, and B. Smit, *Simulating the critical behaviour of complex fluids*, Nature 365 (1993), pp. 330–332.

[31] J.T. Bosko, B.D. Todd, and R.J. Sadus, *Internal structure of dendrimers in the melt under shear: a molecular dynamics study*, J. Chem. Phys. 121(2) (2004), pp. 1091–1096.

[32] J.T. Bosko, *Molecular simulation of dendrimers under shear*, PhD thesis, Swinburne University of Technology, 2005.

[33] G.S. Grest and K. Kremer, *Molecular dynamics simulations for polymers in the presence if a heat bath*, Phys. Rev. A 33(5) (1986), pp. 3628–3631.

[34] K. Kremer and G.S. Grest, *Dynamics of entangled linear polymer melts: a molecular-dynamics simulation*, J. Chem. Phys. 92(8) (1990), pp. 5057–5086.

[35] R. Faller, *Influence of Chain Stiffness on Structure and Dynamics of Polymers in the Melt*, PhD thesis, Johannes Gutenberg-Universität in Mainz, 2000.

[36] R. Faller, F. Muller-Plather, and A. Heuer, *Local reorientation dynamics of semiflexible polymers in the melt*, Macromolecules 33(17) (2000), pp. 6602–6610.

[37] C.F. Abrams and K. Kremer, *The effect of bond length on the structure of dense bead-spring polymer melts*, J. Chem. Phys. 115(6) (2001), pp. 2776–2785.

[38] C.F. Abrams and K. Kremer, *Effects of excluded volume and bond length on the dynamics of dense bead-spring polymer melts*, J. Chem. Phys. 116(7) (2002), pp. 3162–3165.

[39] T.A. Hunt, *Theory and Simulation of Polymer Liquids Under Extensional and Shear Flows*, PhD thesis, Swinburne University of Technology, 2008.

[40] J.D. Weeks, D. Chandler, and H.C. Anderson, *Role of repulsive forces in determining the equilibrium structure of simple liquids*, J. Chem. Phys. 54(12) (1971), pp. 5237–5247.

[41] J.T. Bosko, B.D. Todd, and R.J. Sadus, *Molecular simulation of dendrimers and their mixtures under shear: comparison of isothermal–isobaric (NpT) and isothermal–isochoric (NVT) ensemble systems*, J. Chem. Phys. 123 (2005), 034905.

[42] B.D. Todd and P.J. Daivis, *Homogeneous non-equilibrium molecular dynamics simulations of viscous flow: techniques and applications*, Mol. Simul. 33 (2007), pp. 189–229.

[43] P. Padilla and S. Toxvaerd, *Simulating shear flow*, J. Chem. Phys. 104(15) (1996), pp. 5956–5963.

[44] K.P. Travis and D.J. Evans, *On the rheology of* n*-eicosane*, Mol. Simul. 17 (1996), pp. 157–164.

[45] C. Braga and K.P. Travis, *A configurational temperature Nose–Hoover thermostat*, J. Chem. Phys. 123 (2005), 134101.

[46] A.W. Lees and S.F. Edwards, *The computer study of transport processes under extreme conditions*, J. Phys. C 5 (1921), p. 1972.

[47] M.P. Allen and D.T. Tildesley, *Computer Simulation of Liquids*, Clarendon Press, Oxford, 1987.

[48] C.W. Gear, *Numerical Initial Value Problems in Ordinary Differential Equations*, Prentice-Hall, Englewood Cliffs, NJ, 1971.
[49] M. Doi and S.F. Edwards, *The Theory of Polymer Dynamics*, Oxford University Press, Oxford, 1986.
[50] K. Weissenberg, *A continuum theory of rheological phenomena*, Nature 159 (1947), pp. 310–311.
[51] M.H. Wagner, H. Bastian, P. Hachmann, J. Meissner, S. Kurzbeck, and F. Langouche, *The strain-hardening behaviour of linear and long-chain-branched polyolefin melts in extensional flows*, Rheol. Acta 39 (2000), pp. 97–109.
[52] S.R. de Groot and P. Mazur, *Non-equilibrium Thermodynamics*, North Holland, Amsterdam, 1962.
[53] R.A. Horn and C.R. Johnson, *Matrix Analysis*, Cambridge University Press, Cambridge, 1985.
[54] M. Kröger, *Models for Polymeric and Anisotropic Liquids*, Springer, Berlin, 2005.